Kummerow, J., Spangenberg, E. (2011): Experimental evaluation of the impact of CO2-SO2-brine-reservoir rock interactions on petrophysical properties: A case study from the Ketzin test site, Germany. - Geochemistry Geophysics Geosystems (G3), 12, Q05010

DOI: 10.1029/2010GC003469

Geochemistry Geophysics Geosystems G3

Article
Volume 12, Number 5
1 May 2011
Q05010, doi:10.1029/2010GC003469
ISSN: 1525-2027

Published by AGU and the Geochemical Society

Experimental evaluation of the impact of the interactions of CO_2-SO_2, brine, and reservoir rock on petrophysical properties: A case study from the Ketzin test site, Germany

Juliane Kummerow and Erik Spangenberg

Reservoir Technologies Section, German Research Centre for Geosciences, Telegrafenberg E223, D-14473 Potsdam, Germany (juliane.kummerow@gfz-potsdam.de)

[1] The objective of this study is to evaluate the impact of impure CO_2 on a possible CO_2 repository. Here we present experimental data on the simulation of the injection of pure CO_2 and CO_2 and cocontaminant SO_2 into a saline aquifer. Long-term exposure experiments with pure CO_2 reveal no significant changes in the petrophysical properties (electrical resistivity, elastic wave velocity, and permeability). In contrast, for the injection of CO_2 and cocontaminant SO_2 (1 vol %) we have observed significant and irreversible changes of all monitored physical parameters. On the one hand, the decrease of *P* wave velocity and the increase of electrical resistivity indicate a dissolution of some framework material. On the other hand, the decrease of permeability points to the mobilization and redistribution of fines. These data might be relevant for subsequent modeling and estimations about tolerable concentration limits regarding the contaminants of CO_2 to be stored.

Components: 5300 words, 5 figures, 3 tables.

Keywords: injection of impure CO_2; fluid-rock interactions; resistivity; ultrasonic; velocities; permeability.

Index Terms: 5102 Physical Properties of Rocks: Acoustic properties; 5109 Physical Properties of Rocks: Magnetic and electrical properties (0925); 5114 Physical Properties of Rocks: Permeability and porosity.

Received 10 December 2010; **Revised** 18 March 2011; **Accepted** 29 March 2011; **Published** 19 May 2011.

Kummerow, J., and E. Spangenberg (2011), Experimental evaluation of the impact of the interactions of CO_2-SO_2, brine, and reservoir rock on petrophysical properties: A case study from the Ketzin test site, Germany, *Geochem. Geophys. Geosyst.*, *12*, Q05010, doi:10.1029/2010GC003469.

1. Introduction

[2] CO_2 capture and storage (CCS) in geological formations is considered as a mitigating approach to meet middle- to long-term targets in reducing anthropogenic CO_2 emission [*International Energy Agency*, 2004; *Intergovernmental Panel on Climate Change*, 2005]. Combustion technologies like the Oxyfuel method and coal gasification in combination with purification procedures such as amine gas treatment or cryogenic liquefaction are aimed to produce CO_2 as pure as possible. However, the CO_2 aerated flue gas contains still at least 1 to 2% of contaminants, e.g., N_2, Ar, O_2, SO_2, and NO_x. Generally the cleaning of CO_2 is costly and will reduce the efficiency of a power plant significantly [e.g., *Kather and Scheffknecht*, 2009]. While from a chemical point of view, no critical interactions on fluids and rocks are expected for Ar and N_2 the contaminants SO_2, NO_x and O_2 may have a

Table 1. The pK_S Values at 25°C[a]

Acid	Base	pK_S
H_2SO_4	HSO_4^-	−3.00
HNO_3	NO_3^-	−1.37
H_2SO_3	HSO_3^-	+1.90
$CO_2 + H_2O$	HCO_3^-	+6.35

[a]After *Riedel* [2004] ($pK_S = -\lg K_S$).

considerable impact on the integrity of reservoir and caprocks. Many aspects of the influence of pure CO_2 on formation water and reservoir/caprocks have been studied. Our own research as well as published studies, show that at least quartz-rich sandstones are not altered significantly, and the amount of newly formed minerals is quite small [*Spangenberg and Borm*, 2001; *Schütt et al.*, 2005; *Förster et al.*, 2006; *Xue and Lei*, 2006]. To our knowledge, hardly any data are publicly available which describe the influence of SO_2 and NO_x dissolved in formation water on geological CO_2 repositories. Only some modeling studies have been published, but without any experimental validation [*Knauss et al.*, 2005; *Xu et al.*, 2007]. While CO_2 forms just a weak acid with water (Table 1), SO_2 and NO_x have higher water solubilities, dissociate more easily, and, thus, form strong acids (sulfurous acid, sulfuric acid, nitric acid). Hence, even though SO_2 and NO_x occur only in small concentrations in the flue gas they should have, at least theoretically, a much stronger impact on the rock components than that of carbonic acid. It is also known that the solubility of sulfates in water is mostly lower than that of carbonates. Both dissolution and precipitation of minerals can strongly change the critical reservoir properties, porosity and permeability [*Johnson et al.*, 2001; *Xu et al.*, 2004; *Schütt et al.*, 2005; *Li et al.*, 2006; *Le Guen et al.*, 2007].

[3] Since 2004 the first European on shore research storage test site has been operated in Ketzin (Brandenburg, Germany) to study CO_2 storage in a terrestrial saline aquifer. Currently, food grade CO_2 is injected into the reservoir. However, discussions are ongoing to inject flue gas captured from an Oxyfuel pilot power plant directly. Besides CO_2, these gases also contain SO_2 and NO_x. For this reason we have investigated the impact of pure and impure CO_2 on the petrophysical parameters of a sample from the Ketzin reservoir horizon. Here, we report on the experimental results of interactions between CO_2, brine, and rock and between CO_2-SO_2, brine, and rock. The effect of pure and impure CO_2 injection on the sample is monitored by electrical resistivity, ultrasonic velocity, and permeability measurements, which are sensitive to structural variations in the sample such as changes of pore space and the rock matrix.

2. Rock Characteristics

[4] The experiments were carried out on sample B2-3b from a reservoir sandstone of the Ketzin test site (Upper Triassic Stuttgart formation). The sample used is 49.45 mm in length and 47.6 mm in diameter and was cored from the Ketzin well Ktzi 202/2007 at 629 m depth. It is fine grained and contains predominantly angular fragments of quartz and feldspar embedded in a clay-rich, ferritic matrix (Table 2). Quartz and feldspar are often coated by iron oxides. Partially, the material is cemented by anhydrite and dolomite. The sample has a porosity of 28.07%. In thin sections the distribution of porosity is inhomogeneous with less porous lenticular clay layers and porous grain supported sandstone layers. The lithology of the Ketzin reservoir is described in more detail by *Förster et al.* [2010]. To mimic reservoir conditions, the sample was saturated with a synthetic formation brine composed of 215.27 g/l NaCl, 6.37 g/l $CaCl_2$, 3.96 g/l $MgSO_4$, 1.28 g/l Na_2SO_4, 0.67 g/l KCl (σ = 22.8 S/m at 25°C).

3. Experimental Setup and Methodology

3.1. Apparatus

[5] The flow experiments were performed in the Field Laboratory Experimental Core Analysis System FLECAS [*Kulenkampff and Spangenberg*, 2005] at simulated conditions of the Ketzin reservoir (p_{conf} = 15 MPa, p_{pore} = 7.5 MPa, and T = 40°C).

Table 2. XRD Analyses of the Original Sample Material and of the Sample After the CO_2-SO_2 Experimental Cycle[a]

Component	Original Material: Volume Fraction (wt %)	After CO_2SO_2 Exposure: Volume Fraction (wt %)
Quartz	39.3 ± 2.0	42.0 ± 2.0
Albite	31.6 ± 2.2	33.0 ± 2.2
Orthoclase	7.4 ± 1.1	8.5 ± 1.2
Dolomite	2.8 ± 0.5	1.5 ± 0.6
Anhydrite	4.5 ± 1.0	–
Illite	10.9 ± 1.4	10.7 ± 1.4
Hematite	2.1 ± 0.2	2.5 ± 0.3
Halite	1.4 ± 0.2	1.9 ± 0.2

[a]Errors are absolute errors.

Table 3. *P* Wave Velocities and Volume Fractions[a]

Component	V_P (m/s)	Original Material: Volume Fraction (%)	After CO_2SO_2 Exposure: Volume Fraction (%)
Quartz	6030	0.2830	0.2846
Albite	5940	0.2275	0.2236
Orthoclase	5630	0.0533	0.0576
Dolomite	3500	0.0202	0.0102
Anhydrite	5620	0.0324	0.0000
Clay	4320	0.0785	0.0725
Hematite	6510	0.0151	0.0169
Halite	4560	0.0101	0.0129
Pores (brine filled)	1780	0.2800	0.3224
Σ		0.9994	0.9991

	V_P Before Experiment (m/s)	V_P After Experiment (m/s)	Decrease of V_P (%)
Reuss model	3493.81	3318.90	5.01
Measured	2999.40	2769.70	7.67

[a]Single crystal *P* wave velocities and volume fractions of the rock forming minerals are used to model the velocities of the sample before and after the CO_2-SO_2 experimental cycle. The volume fractions account for the sample porosity. The *P* wave velocities of the single crystals are taken from *Gebrande* [1982] and *Eastwood and Castagna* [1987]. The *P* wave velocity of the pore fluid was calculated after *Batzle and Wang* [1992]. The Reuss model was applied because in the experiment the velocities were measured normal to the bedding planes.

The system consists of an internally heated oil pressure vessel, capable of a maximum confining pressure, p_{conf}, of 70 MPa and a maximum working temperature of 250°C (Figure 1a). Confining and pore pressures are controlled by syringe pumps (ISCO 100DM and ISCO 500DM, respectively). The pore fluid pressure system is operated by a total of three pumps. On the upstream side two pumps deliver brine and supercritical CO_2 ($scCO_2$) to the system at constant flow rates while the downstream pump is kept in constant pressure mode. The whole pore pressure system (pumps, valves, capillaries) is embedded in a thermal insulation system and heated up to the experimental working temperature of 40°C. Equalization of the temperatures in the pumps and sample allows for reliable monitoring of flow rates and flow volumes displayed by the pump controllers. Furthermore, the heating of the pumps is essential to reach the stability field of $scCO_2$.

[6] To minimize the risk of corrosion of the syringe pumps in the flow experiment with $scCO_2$-SO_2 the gas mixture was preconditioned in a heated media separator using the upstream CO_2 pump for pressurization (Figure 1b).

3.2. Specimen Setup, Data Acquisition, and Processing

[7] The cylindrical rock sample (47.6 mm in diameter and 49.45 mm in length) is placed between end caps made of Hastelloy (Figure 2). Sample and end caps are jacketed with a PFA (perfluoralkoxy) heat shrinkable tubing. The end caps contain the pore pressure port, ultrasonic *P* and *S* wave transducers and act as electrodes. Hence, the specimen setup allows for the combined measurement of the hydraulic, electric, and elastic rock parameters.

3.2.1. Permeability Measurements

[8] The brine permeability, *k*, of the Ketzin reservoir sample was determined using Darcy's law [e.g., *Darcy*, 1856; *Scheidegger*, 1974]:

$$k(p_{conf}, p_{pore}) = \frac{Q \cdot l \cdot \eta(T_s, p_{pore})}{\Delta p} \cdot \frac{1}{\pi r^2}, \qquad (1)$$

where Q is the flow rate, l is the length of the sample, η is the fluid viscosity, Δp is the pressure difference, and r the sample radius.

[9] Pumps, capillaries, and valves were heated to the reservoir temperature of 40°C. Therefore, no

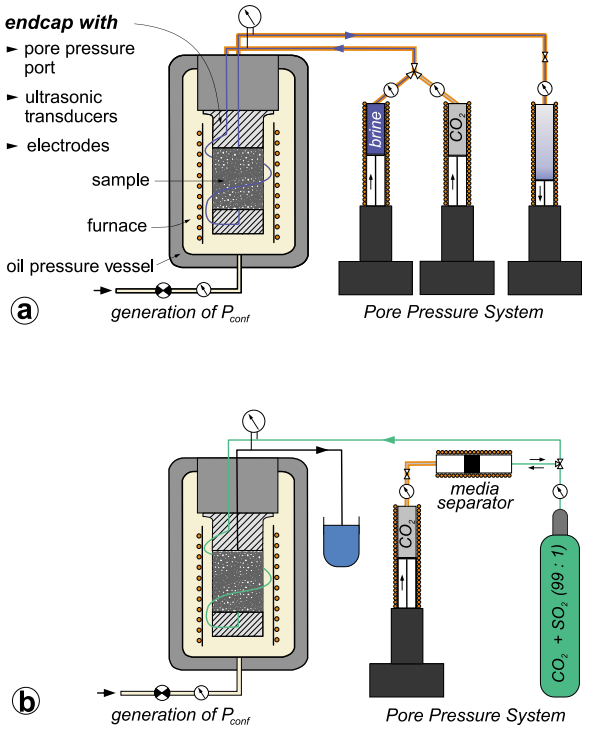

Figure 1. Experimental setups for (a) long-term two-phase flow experiments using CO_2 and brine at different ratios and (b) water alternating gas (WAG) tests with brine and a CO_2-SO_2 mixture.

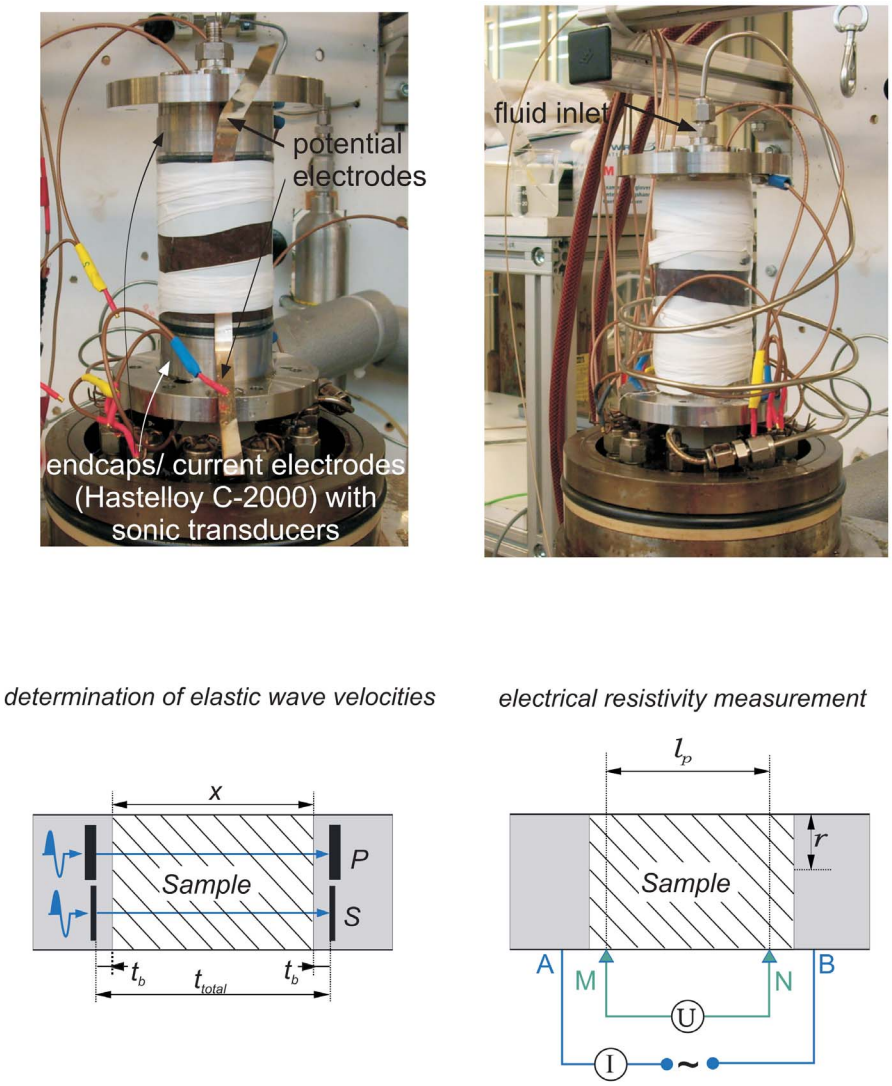

Figure 2. Measuring arrangements for the determination of elastic wave velocities and electrical resistivity.

corrections for temperature- and pressure-dependent molar volumes were necessary. The fluid viscosity, η (T_s, p_{pore}), at the pore pressure and sample temperature was taken from *Lemmon et al.* [2010].

3.2.2. Ultrasonic Measurements

[10] Ultrasonic measurements were performed in the pulse transmission mode at a resonance frequency of 500 kHz. The signals were recorded after at least 30 min were given for the samples to adjust to the experimental pressure and temperature conditions.

[11] The traveltimes were corrected for the dead time, t_d, of the recording device (transducer, function generator, oscilloscope) and the traveltime through the end caps, t_b, which were determined at ambient conditions. Changes in the sample length, l, due to increasing pressure cannot be measured directly during the experiment. Therefore, a correction is made from determined velocities v_p, v_s, and the rock density, ρ_0, at 1 bar, using an approximation based on *Gebrande* [1982]:

$$\frac{l(P)}{l_0} = \left[1 + \frac{1}{\rho_0}\int_0^P \left(\frac{1}{v_p^2 - \frac{4}{3}v_s^2}dP\right)\right]^{-\frac{1}{3}}, \qquad (2)$$

where l_0 is the initial sample length.

3.2.3. Determination of Resistivity

[12] The sample resistivity was measured with a four electrode arrangement (Figure 2). The end caps act as current electrodes *A* and *B* to which a 1 kHz AC voltage with an amplitude of 1 V is applied. The

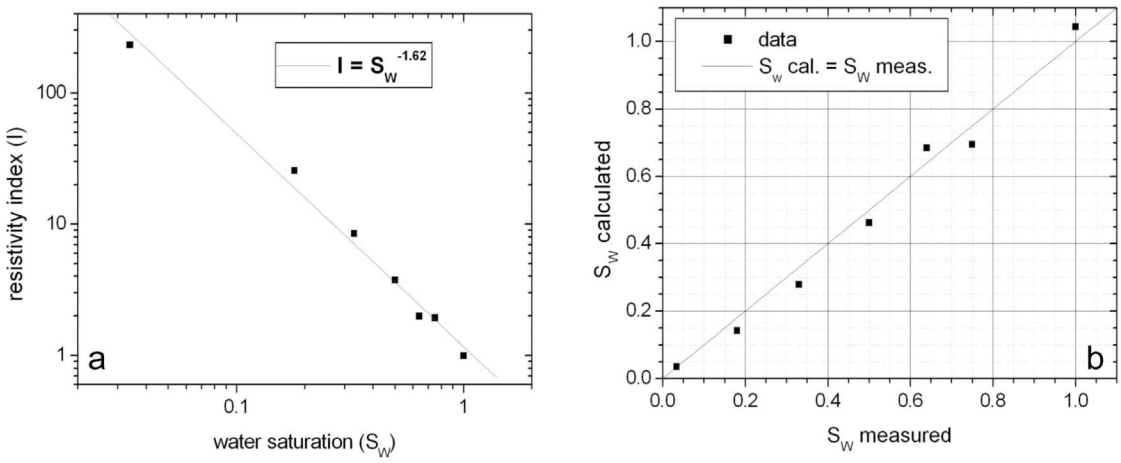

Figure 3. (a) Resistivity index versus water saturation and (b) the comparison of measured water saturation and values estimated with Archie's 2nd equation and n = 1.62.

voltage drop is recorded between two silver electrodes (M and N) that are attached to the sample surface and contacted through the PFA jacket. The potential is monitored with a scanning data acquisition system (Agilent 34970A). The resistivity, ρ_s, is calculated from:

$$\rho_s[\Omega m] = R \cdot \frac{A}{d_e}, \tag{3}$$

where R is the resistance, A is the cross-sectional area of the sample and d_e is the distance between the potential electrodes M and N.

3.2.4. Determination of Water Saturation

[13] Since we have no opportunity for a direct determination of water saturation of the sample during the experiments in the high-pressure cell, we determined the saturation exponent for the sample under ambient conditions. This provides the possibility to estimate the water saturation from resistivity measurements based on Archie's 2nd equation:

$$\frac{\rho_t}{\rho_0} = I = S_W^{-n}, \tag{4}$$

where ρ_0 is the resistivity of the fully brine saturated sample and ρ_t the resistivity at partial saturation. The determined saturation exponent of n = 1.62 is low compared with the average value of 2 for sandstones. This low value is most likely caused by the high clay content of about 11%. Figure 3 shows the resistivity index versus water saturation in a log-log plot and the comparison of the measured water saturation with the values that result from the application of Archie's 2nd equation with n = 1.62. The maximum error in the saturation estimation is 5.4%. However, the application of a calibration under ambient condition for an experiment under simulated in situ pressure involves the uncertainty that the estimation error might increase, since the electrical properties depend to a certain degree on pressure. The uncertainty of this approach will further increase when fluid-rock interaction causes changes of the structure of the fluid rock interface and the pore microstructure.

4. Experimental Procedure and Results

[14] The flow experiments were conducted over periods of 2 and 4 weeks at constant pressure and temperature, simulating the conditions of the Ketzin reservoir. After the in situ confining pressure, p_{conf}, of 15 MPa was applied, the temperature, T, was increased to 40°C. When temperature equilibrium was reached, a vacuum was applied to the sample via one pore pressure port and formation brine was sucked into the sample via the second pore pressure port. After completion of the sample saturation the pore pressure, p_{pore}, was adjusted to 7.5 MPa.

4.1. Flow Experiment With Formation Brine and CO_2

[15] Pure $scCO_2$ was injected in the completely brine saturated sample for 166 h (~7 days). After 48 h the flow rate was reduced from 0.4 ml/min to 0.2 ml/min to reduce the risk of mobilization of fines. The resaturation with brine (imbibition) was performed as a two-phase flow experiment, whereby the flow rate of the brine was successively increased by 0.05 ml/min at a constant flow rate of the $scCO_2$ stream. The pore volume was exchanged at least

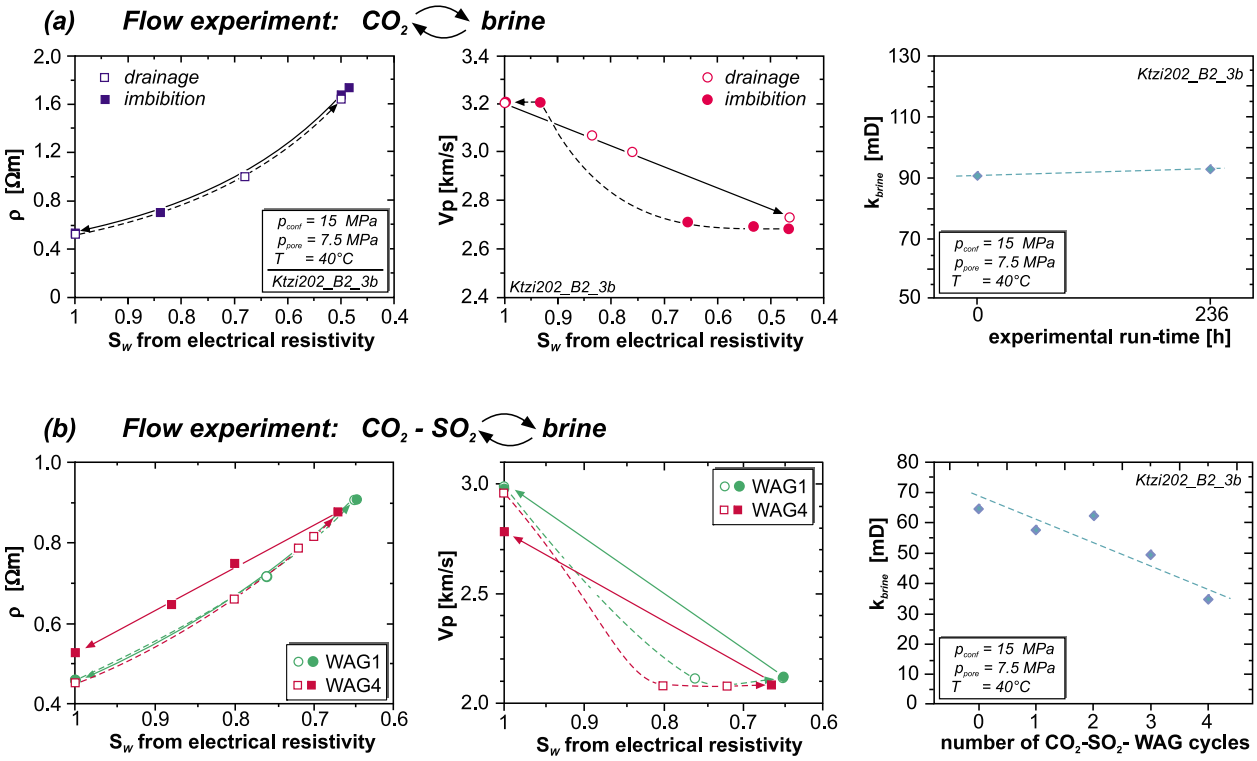

Figure 4. Electrical resistivity ρ and P wave velocity v_p as functions of the brine saturation S_W of the sample. The permeability k_{brine} was determined at the beginning and the end of the flow cycles. (a) CO_2-brine flow and (b) CO_2-SO_2-brine flow.

20 times before the flow ratio (brine: CO_2 ratio) was changed. Prior to the change of flow ratio the P and S wave velocities were measured and the electrical resistivity was determined. The permeability was measured before the $scCO_2$ injection and again after a complete imbibition with brine was achieved and no further changes in petrophysical parameters occur (after 6 days of pure brine flow).

[16] The S wave velocity increases with decreasing brine saturation from 1.38 km/s to 1.40 km/s, what accounts only for a velocity change of about 2%. This is primarily due to the decreasing sample density with decreasing brine saturation. The measured resistivity and P wave velocity versus brine saturation are shown in Figure 4a. As CO_2 is nonconductive, the charge transfer in the sample is primarily bound to the formation pore fluid. Hence, the resistivity increases with decreasing brine saturation from 0.54 Ωm to 1.73 Ωm and decreases when the sample is brine flooded again. The P wave velocities v_p show an hysteretic behavior resulting from a relative rapid decrease of v_p with decreasing brine saturation from 3.20 km/s to 2.69 km/s and a hesitant increase of v_p at brine imbibition. Both, the resistivity and P wave velocity reach their initial values after the sample is resaturated with brine at the end of the experiment. We observe a minimal increase of the permeability at the end of the experiment from 90.25 mD to 92.01 mD. However, this is most probably related to the mobilization of clay minerals, which were found in the capillaries after the experiment was finished.

[17] At the end of the experiment we had to carry out some maintenance work at the system and to install the media separator in the fluid pressure system, so the sample had to be taken out of the system carefully. We cleaned the sample cautiously from salt precipitations and kept it saturated in a closed container with synthetic formation water for the following experiment.

4.2. Flow Experiment With Formation Brine Alternating CO_2-SO_2

[18] Reaction fluids of experiments with $scCO_2$ + SO_2 (99.5 + 0.5 vol %) have a pH between 2 and 3, when they are in contact with silicate phases [*Erzinger et al.*, 2010]. We expect a similar pH value for the flow experiment with a mixture of 99% CO_2 and 1% SO_2. Thus, to minimize the corrosion risk of the experimental facility due to the higher acidity of the CO_2-SO_2 mixture, we

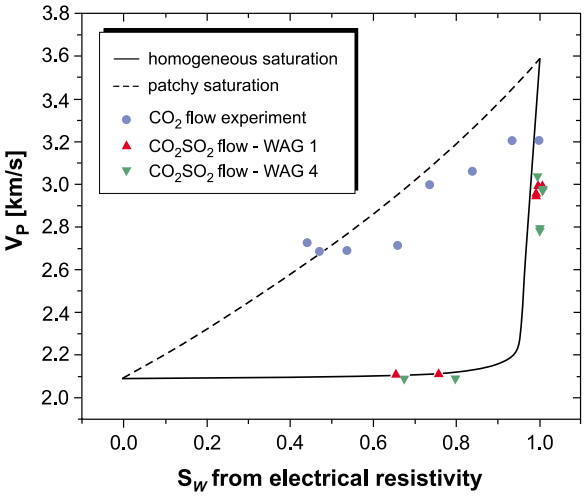

Figure 5. Fluid substitution models for a homogeneous and patchy saturation. Blue solid circles represent measured v_p data during a CO_2 flow experiment, and red and green triangles indicate data points recorded during the first and the fourth WAG cycles of the CO_2-SO_2 flow experiment, respectively.

have performed four shorter WAG cycles (water alternating gas). The experiment was started with pure brine at a flow rate of 0.2 ml/min. Then, the brine flow was stopped and the preconditioned $scCO_2$-SO_2 mixture was injected into the sample. After a maximum 65.5 h of constant flooding, the sample was resaturated with pure formation brine. In total, the sample was $scCO_2$-SO_2 flooded for 117.5 h.

[19] No interpretable *S* wave data are available for this run as we had an accidental ground almost from the beginning of the experiment. After passing four complete WAG cycles the electrical resistivity at complete brine saturation increases by 16.26%, while the *P* wave velocity and the permeability decrease by 7.67% and 45.97%, respectively (Figure 4b). The changes in the determined petrophysical properties are irreversible. The sample surface shows a greenish discoloring when the sample is disassembled. Since the sample is poorly consolidated and sanding during handling, it was not possible to determine the porosity change.

5. Discussion

[20] The effect of the injection of supercritical CO_2 and CO_2-SO_2 in a brine saturated reservoir rock sample from the Ketzin CO_2 sequestration site on permeability, electrical resistivity, and ultrasonic velocities has been investigated at simulated in situ conditions (p_{conf} = 15 MPa, p_{pore} = 7.5 MPa, and T = 40°C) over periods of 2 and 4 weeks, respectively. Our study shows a strong distinction between flow experiments conducted with pure CO_2 and that performed with a CO_2-SO_2 mixture. After exposing the Ketzin reservoir sample to pure supercritical CO_2 for 236 h the variations of the measured physical rock properties are reversible and provide no indications of mineral reactions.

[21] In contrast, the reservoir rock is highly affected by the injection of supercritical CO_2-SO_2. This is reflected by the discoloring of the sample as well as by the considerable changes of the intrinsic physical rock properties. The irreversible reduction of the *P* wave velocity after 117.5 h of CO_2-SO_2 flooding indicates a degradation of the rock's frame modulus possibly due to the dissolution of, e.g., grain cement. In contrast, the increase of electrical resistivity and the decrease of permeability point to a reduction of the transport efficiency of the pore network. Since we have no evidence for precipitation of new solid phases we interpret the decrease as a result of fines mobilization and redistribution in the porous system. In this situation, the relocated fines decrease the efficiency for charge and fluid transport but did not contribute to a stiffening of the frame modulus. There is no indication for a precipitation of new minerals from XRD analyses (Table 2). But, in the CO_2-SO_2 exposed sample the dolomite fraction is lower compared to that in the original material and the anhydrite is missing completely, while all other phases remain more or less constant. This could be a hint for mineral dissolution. From single crystal *P* wave velocities of the rock-forming minerals and their volume fractions in the sample *P* wave velocities were calculated for the original and the sample after CO_2-SO_2 exposure. The modeled velocity reduction is on the order of the measured one (Table 3). However, as the samples analyzed with XRD could not be the same for technical reasons, we cannot exclude the influence of sample heterogeneities.

5.1. Fluid Substitution Modeling

[22] On the basis of the measured velocity data fluid substitution models for a homogeneous (Gassmann) and a patchy fluid distribution [*Kazemeini et al.*, 2010] were calculated (Figure 5). *Gassmann*'s [1951] relation has been used for the modeling in the following form:

$$K_{sat} = K_{dry} + \frac{\left(1 - \frac{K_{dry}}{K_{matrix}}\right)^2}{\frac{\phi}{K_{fluid}} + \frac{(1-\phi)}{K_{matrix}} - \frac{K_{dry}}{K_{matrix}^2}}, \qquad (5)$$

where ϕ is the sample porosity and K_{matrix}, K_{dry}, and K_{fluid} are the bulk moduli of the matrix material, the dry rock skeleton and the pore fluid, respectively. K_{matrix} was calculated considering the mineralogical composition of the rock material (see Table 2). The modulus of the brine (215 g/l NaCl) has been calculated for in situ conditions based on the equation of *Batzle and Wang* [1992]. The modulus of CO_2 and the densities of CO_2 and water have been taken from the NIST database. The density of the composite fluid was calculated with

$$\rho_{fluid} = \rho_{brine} S_W + (1 - S_W)\rho_{CO_2}, \quad (6)$$

and the density of the saturated rock is given by

$$\rho_{sat} = \rho_{fluid}\phi + (1 - \phi)\rho_{matrix}. \quad (7)$$

The patchy model was calculated following the approach of *Kazemeini et al.* [2010] which is based on the works of *Hill* [1963] and *Berryman and Milton* [1991]:

$$K_{patchy} = \left[\sum_{i=1}^{n} \frac{x_i}{\left(K_i + \frac{4}{3}G\right)}\right]^{-1} - \frac{4}{3}G, \quad (8)$$

where n is the number of patches with different fluid content, x_i is the volume fraction of the ith patch, K_i is the bulk modulus of the rock completely saturated with the ith fluid, and G is the shear modulus of the rock.

[23] At least the data of the CO_2 flow experiment do not fit the Gassmann model. Rather, they follow the trend of a patchy saturation model. The velocity for the saturated sample is below the model prediction. This is possibly due to the high clay content of the Ketzin reservoir of about 11%, because in water-saturated clay containing rocks often a "weakening" of the frame moduli occurs and thus one assumption of fluid substitution models is not fulfilled. From the observed velocity trend we assume that the transport of the pure CO_2 through the sample occurs via the permeable flow path ways in the sandy portions of the sample, while large patches of the sample remain fully brine saturated presumably due to the higher capillarity and lower permeability in the fine pored clay-rich layers.

[24] For the CO_2-SO_2 flow experiment the P wave velocity is 6.5% lower at complete brine saturation than it was determined for the flow experiment with pure CO_2 (Figure 5). After the last velocity measurement of the first experiment the sample properties might have been influenced by (1) stress relaxation after the sample was brought back to room pressure and temperature; (2) the cleaning from salt precipitations and resaturation; and (3) the following installation, pressurization and heating to in situ conditions for the second experiment.

[25] We will not speculate which of these influences in combination with the clay mobilization during the first flow experiment might be the domination effect, however, for the second flow experiment the sample shows a different behavior of seismic properties. The wave velocities rather fit the Gassmann model, after already one WAG cycle with CO_2-SO_2.

5.2. Supercritical CO_2 Drying

[26] For the adjusted flow rates we did not observe a "drying effect" of supercritical CO_2 or CO_2-SO_2 in the electrical measurements as a minimum brine saturation of 47% was attained. Although supercritical CO_2 has the ability to dissolve water, it requires much longer experimental time or/and much higher flow rates to produce a clear "drying effect" in this type of rock for the following reasons:

[27] 1. Thin section analysis shows areas of permeable open or clay free pores accessible for brine displacement by CO_2 and clay filled areas, which very likely remain water saturated. This patchy saturation distribution is supported by the dependence of the P wave velocity on saturation (see Figure 5).

[28] 2. The displacement of the water in this clay-free pore network by $scCO_2$ causes a certain decrease in the rock resistivity. The remaining bound water is now accessible for dissolution in the $scCO_2$ at the CO_2-brine interface. The dissolution process results in a decrease of the thickness of the bound water layer and an increase of the bound water salinity. As long as the solubility limit is not reached and no precipitation of salt occurs, this will not have a significant effect on the electrical resistivity of the drained pore network as the number of free charge carrier remains constant.

[29] 3. The clay-filled water saturated patches form a conductive network and are responsible for the remaining low resistivity of the partially saturated rock. Because the ratio of CO_2-brine interface to brine volume of these water saturated clay-filled patches is much smaller than that of the bound water CO_2 interface in the clay-free pore network, the drying of these patches by $scCO_2$ occurs on order of magnitude longer time scale.

[30] 4. However, the high residual water saturation and the low rock resistivity is a result of the clay content. Even if we get/have salt precipitation in the already drained clay-free pore network, we cannot expect a strong effect on the overall low rock resistivity.

6. Conclusion

[31] This study shows that the injection of $scCO_2$-SO_2 into the Ketzin reservoir formation changes considerably the critical reservoir properties. In a real injection case the impact of fluid-rock interactions is expected to be greatest in the vicinity of the injection point, and to have an adverse effect on the long-term injection performance.

[32] Fluid-rock interactions are generally very complex and CO_2 exposure experiments in batch reactors show that the alteration of minerals and/or the precipitation of new ones depend on a variety of parameters: pressure and temperature, rock composition, fluid chemistry, structural parameters, such as porosity, pore space structure, internal reaction surface, permeability, and time [*Schütt et al.*, 2005; *Wigand et al.*, 2008]. Consequently, more data are needed in the future to cover the broad spectrum of different reservoir types. Furthermore, a sufficient amount of sample material is necessary in order to compare the impact of different influences and parameters, which cannot always be provided within the site specific demonstration projects with only limited amount of core material. Besides this, an improvement of the methodology by the combination of the state-of-the-art petrophysical measurements with the visualization techniques like μCT monitoring, NMR technique, etc, is required to increase the significance and reliability of interpretation.

Acknowledgments

[33] We would like to thank the CO_2Sink group for providing us with the sample material and Rudolf Naumann for performing XRD analyses. Andreas Kratz, Rainer Becker, and Mathias Kreplin are thanked for the sample preparation, and Ronny Giese is thanked for the technical support. We are grateful to J. Kuhlenkampff and two anonymous referees for their constructive and motivating reviews. This study is part of the COSONOStRA ("CO_2-SO_2-NO_x Stimulated Rock Alteration") project, funded by the Programme "Geotechnologien" of the German Federal Ministry of Education and Research (grant 03G0685A, publication GEOTECH-1553).

References

Batzle, M., and Z. Wang (1992), Seismic properties of pore fluids, *Geophysics*, *57*(11), 1396–1408, doi:10.1190/1.1443207.

Berryman, J. G., and G. W. Milton (1991), Exact results for generalized Gassmann's equation in composite porous media with two constituents, *Geophysics*, *56*, 1950–1960, doi:10.1190/1.1443006.

Darcy, H. (1856), *Les Fontaines Publiques de la Ville de Dijon*, Dalmont, Paris.

Eastwood, R. L., and J. P. Castagna (1987), Interpretation of V_p/V_s ratios from sonic logs, in *Shear Wave Exploration*, *Geophys. Dev. Ser.*, vol. 1, edited by S. H. Danbom and S. N. Domenico, pp. 139–153, Soc. of Explor. Geophys., Tulsa, Okla.

Erzinger, J., F. Wilke, T. Wiersberg, and M. Vasquez Parra (2010), Experimental studies on the interaction of $scCO_2$ and $scCO_2$-SO_2 with rock forming minerals at conditions of geologic carbon storages—First results, Abstract GC31B-0874 presented at 2010 Fall Meeting, AGU, San Francisco, Calif., 13–17 Dec.

Förster, A., et al. (2006), Baseline characterization of the CO2-SINK geological storage site at Ketzin, Germany, *Environ. Geosci.*, *13*(3), 145–161, doi:10.1306/eg.02080605016.

Förster, A., R. Schöner, H.-J. Förster, B. Norden, A.-W. Blaschke, J. Luckert, G. Beutler, R. Gaupp, and D. Rhede (2010), Reservoir characterization of a CO_2 storage aquifer: The Upper Triassic Stuttgart Formation in the Northeast German Basin, *Mar. Pet. Geol.*, *27*, 2156–2172, doi:10.1016/j.marpetgeo.2010.07.010.

Gassmann, F. (1951), Über die Elastizität poröser Medien, *Vierteljahresschr. Natur-forsch. Ges. Zuerich*, *96*, 1–23.

Gebrande, H. (1982), Elastic wave velocities and constants of elasticity of rocks and rock-forming minerals, in *Landolt-Börnstein: Zahlenwerte und Funktionen aus Naturwissen-schaften und Technik*, *New Ser.*, vol. 1b, edited by G. Angenheister, pp. 1–99, Springer, Berlin.

Hill, R. (1963), Elastic properties of reinforced solids: Some theoretical principles, *J. Mech. Phys. Solids*, *11*, 357–372, doi:10.1016/0022-5096(63)90036-X.

Intergovernmental Panel on Climate Change (2005), *IPCC Special Report on Carbon Dioxide Capture and Storage*, edited by B. Metz et al., Cambridge Univ. Press, Cambridge, U. K.

International Energy Agency (2004), *Prospects for CO_2 Capture and Storage*, 249 pp., Paris.

Johnson, J. W., J. J. Nitao, C. J. Steefel, and K. G. Knauss (2001), Reactive transport modeling of geologic CO_2 sequestration in saline aquifers: The influence of intraaquifer shales and the relative effectiveness of structural, solubility, and mineral trapping during prograde and retrograde sequestration, paper presented at 1st National Conference on Carbon Sequestration, Natl. Energy Technol. Lab., Washington, D. C.

Kather, A., and G. Scheffknecht (2009), The oxycoal process with cryogenic oxygen supply, *Naturwissenschaften*, *96*, 993–1010, doi:10.1007/s00114-009-0557-2.

Kazemeini, S. H., C. Juhlin, and S. Fomel (2010), Monitoring CO_2 response on surface seismic data; a rock physics and seismic modeling feasibility study at the CO_2 sequestration site, Ketzin, Germany, *J. Appl. Geophys.*, *71*, 109–124, doi:10.1016/j.jappgeo.2010.05.004.

Knauss, K. G., J. W. Johnson, and C. I. Steefel (2005), Evaluation of the impact of CO_2, co-contaminant gas, aqueous fluid and reservoir rock interactions on the geologic seques-

tration of CO_2, *Chem. Geol.*, *217*, 339–350, doi:10.1016/j.chemgeo.2004.12.017.

Kulenkampff, J., and E. Spangenberg (2005), Physical properties of cores from the JAPEX/JNOC/GSC et al. Mallik 5L-38 gas hydrate production research well under simulated in situ conditions using the Field Laboratory Experimental Core Analysis System (FLECAS), in *Scientific Results From the Mallik 2002 Gas Hydrate Production Research Well Program, Mackenzie Delta, Northwest Territories, Canada* [CD-ROM], edited by S. R. Dallimore and T. S. Collett, *Bull. Geol. Surv. Can.*, *585*.

Le Guen, Y., F. Renard, R. Hellmann, E. Brosse, M. Collombet, D. Tisserand, and J.-P. Gratier (2007), Enhanced deformation of limestone and sandstone in the presence of high P_{CO2} fluids, *J. Geophys. Res.*, *112*, B05421, doi:10.1029/2006JB004637.

Lemmon, E. W., M. O. McLinden, and D. G. Friend (2010), Thermophysical properties of fluid systems, in *NIST Chemistry WebBook*, *NIST Stand. Ref. Database*, *69*, edited by P. J. Linstrom and W. G. Mallard, http://webbook.nist.gov/chemistry/, Natl. Inst. of Stand. and Technol., Gaithersburg, Md.

Li, R., K. Dodds, A. F. Siggins, and M. Urosevic (2006), A rock physics simulator and its application for CO_2 sequestration process, *Explor. Geophys.*, *37*, 67–72, doi:10.1071/EG06067.

Riedel, E. (2004), *Anorganische Chemie*, 6th ed., 935 pp., de Gruyter, Berlin.

Scheidegger, A. E. (1974), *The Physics of Flow Through Porous Media*, Univ. of Toronto Press, Toronto, Ont., Canada.

Schütt, H., M. Wigand, and E. Spangenberg (2005), Geophysical and geochemical effects of supercritical CO_2 on sandstones, in *Carbon Dioxide Capture for Storage in Deep Geologic Formations—Results From the CO_2 Capture Project*, vol. 2, edited by D. C. Thomas and S. Benson, pp. 767–786, doi:10.1016/B978-008044570-0/50133-1, Elsevier, Amsterdam.

Spangenberg, E., and G. Borm (2001), The influence of CO_2 injection on the physical properties of reservoir and cap rocks, paper presented at SMV Technology Workshop, Potsdam, Germany.

Wigand, M., J. W. Carey, H. Schütt, E. Spangenberg, and J. Erzinger (2008), Geochemical effects of CO_2 sequestration in sandstones under simulated in-situ conditions of deep saline aquifers, *Appl. Geochem.*, *23*(9), 2735–2745, doi:10.1016/j.apgeochem.2008.06.006.

Xu, T., J. A. Apps, and K. Pruess (2004), Numerical simulation of CO_2 disposal by mineral trapping in deep aquifers, *Appl. Geochem.*, *19*, 917–936, doi:10.1016/j.apgeochem.2003.11.003.

Xu, T., J. A. Apps, K. Pruess, and H. Yamamoto (2007), Numerical modeling of injection and mineral trapping of CO_2 with H_2S and SO_2 in sandstone formation, *Chem. Geol.*, *242*, 319–346, doi:10.1016/j.chemgeo.2007.03.022.

Xue, Z., and X. Lei (2006), Laboratory study of CO_2 migration in water-saturated anisotropic sandstone, based on *P* wave velocity imaging, *Explor. Geophys.*, *37*, 10–18, doi:10.1071/EG06010.